

Modeling the long term dynamics of pre-vaccination pertussis

Ganna Rozhnova^{*1,2} and Ana Nunes¹

¹*Centro de Física da Matéria Condensada and Departamento de Física,
Faculdade de Ciências da Universidade de Lisboa,
P-1649-003 Lisboa Codex, Portugal*

²*Kavli Institute for Theoretical Physics, Kohn Hall,
University of California, Santa Barbara, CA 93106-4030*

arXiv:1104.5112v2 [q-bio.PE] 25 Feb 2012

* corresponding author
a_rozhnova@cii.fc.ul.pt

Abstract

The dynamics of strongly immunizing childhood infections is still not well understood. Although reports of successful modeling of several incidence data records can be found in the literature, the key determinants of the observed temporal patterns have not been clearly identified. In particular, different models of immunity waning and degree of protection applied to disease and vaccine induced immunity have been debated in the literature on pertussis. Here we study the effect of disease acquired immunity on the long term patterns of pertussis prevalence. We compare five minimal models, all of which are stochastic, seasonally forced, well-mixed models of infection based on susceptible-infective-recovered dynamics in a closed population. These models reflect different assumptions about the immune response of naive hosts, namely total permanent immunity, immunity waning, immunity waning together with immunity boosting, reinfection of recovered, and repeat infection after partial immunity waning. The power spectra of the output prevalence time series characterize the long term dynamics of the models. For epidemiological parameters consistent with published data for pertussis, the power spectra show quantitative and even qualitative differences that can be used to test their assumptions by comparison with ensembles of several decades long pre-vaccination data records. We illustrate this strategy on two publicly available historical data sets.

Keywords: pertussis, childhood diseases, recurrent epidemics, stochastic fluctuations, power spectra

I. INTRODUCTION

Childhood infections remain a public health as well as a modeling challenge, despite many decades of control measures and theoretical efforts. Large vaccination programmes against some of these diseases started in the 1940s-1960s in the developed countries and led to dramatic reductions of incidence levels, but in the developing countries they are still a cause of significant levels of infant mortality [1–6]. The resurgence of pertussis, also known as whooping cough, reported in developed countries after decades of high vaccine coverage [7–11], as well as a recent upsurge of measles in eastern and southern Africa prompted a renewed interest in assessing the efficacy of control policies for these childhood infections.

Such an assessment must rely on simulations based on mathematical models. The complexity and diversity of the long term dynamics of childhood diseases has been long acknowledged as a major problem in mathematical epidemiology [12–15]. More recent work focused on contact structure, stochasticity and seasonality has brought considerable advances in understanding and selecting some of the fundamental ingredients that drive the observed incidence temporal patterns [16–23] and in developing analytic tools to deal with these ingredients and their interplay with the model’s nonlinearities [24–32].

Models of higher complexity involve many parameters, some of which are difficult to determine, leaving considerable room for data fitting [33–36]. On the other hand, one of the features of childhood infections is the variability exhibited by different data records, even within those that correspond to a single disease in comparable social environments [5, 18, 37]. Therefore, successful modeling of particular sets of incidence data records reported in the literature [18, 38, 39] has not closed the discussion about the key determinants of the observed dynamics. Measles is an exception for which a parsimonious model has been shown to reproduce the behavior of different data sets [16, 40, 41], and it is generally accepted that the disease dynamics in large urban populations is adequately described by a stochastic seasonally forced well-mixed susceptible-infective-recovered (SIR) or susceptible-exposed-infective-recovered based model.

At the opposite extreme, pertussis keeps defying mathematical modeling, as illustrated

by recent efforts in different directions [11, 39, 42–45]. In particular, several proposals explore hypothesis about disease induced and vaccine induced immunity [11, 37, 45], relying on assumptions about vaccine uptake and efficacy for the purpose of comparison with real data. This is a difficult problem of great interest and enormous relevance for public health. However, we are still lacking a sound uncontroverted model for pre-vaccination pertussis.

Here we have sought to contribute to the goal of using pre-vaccination data records to obtain information about the properties of disease induced immunity. The paper focuses on exploring the influence of naive hosts immune response in the long term patterns of pertussis prevalence as given by the averaged power spectra of simulated time series corresponding to several decades. The power spectrum of the stochastic seasonally forced well-mixed SIR model is compared with those of four modifications of the model that reflect different assumptions about disease induced immunity. These four different assumptions have been proposed in the literature in the framework of deterministic models that have all been shown to be compatible with available data. The five variants we consider deliberately avoid all the complications related with contact structure and spatial spread, as well as vaccine coverage and efficacy and waning of vaccine-induced immunity, in order to keep a relatively low number of free parameters in the model.

We show that the stochastic versions of the SIR model and its four variants have significantly different properties, which translate into quantitatively different prevalence and incidence power spectra. This opens the possibility of using the stochastic properties of long, well resolved data records to constrain these and other variants of the model, using the power spectra of the pertussis incidence time series in large urban centers in the pre-vaccination era as the target long term dynamics that the model should reproduce. We illustrate this strategy by applying it to two publicly available historical data records for pre-vaccination pertussis incidence.

II. MODELS AND METHODS

A. Models

We consider five seasonally forced stochastic compartmental models summarized in Fig. 1 as candidates for the description of pre-vaccination pertussis (the deterministic counterparts of these models are described in the Supplementary Material). In all cases, the population includes three classes of individuals, the susceptible [S in (a)-(d), S_1 and S_2 in (e)], the infectious [I in (a)-(c), I_1 and I_2 in (d)-(e)] and the recovered [R in (a)-(b) and (d)-(e), R and W in (c)]. Also in all five cases, there is replenishment through births of susceptible individuals that have never before contracted the disease. The birth rate is kept constant and equals the death rate μ .

1. *SIR model*

Model (a) is the standard SIR model: recovery confers permanent immunity, and all infections are first infections. Infected individuals recover at a constant rate δ , and susceptible individuals are infected at a rate $\lambda_t = \beta(t)I/N$, where N is the population size, I is the number of infected individuals and $\beta(t)$ is a periodic function of period one year that represents the variable contact rate associated with the school terms. For the purpose of studying the long term temporal patterns of the fluctuations of this stochastic process the particular form of $\beta(t)$ is not crucial, and we shall take $\beta(t) = \beta_0(1 + \beta_1 \cos 2\pi t)$.

2. *SIRS model*

Model (b) is the standard SIRS model. It differs from the SIR model in that recovery does not confer permanent immunity. Instead, recovered individuals' immunity wanes at a constant rate γ and then they become susceptible again. The fraction of primary infections is given approximately by $\mu/[\gamma(1 - s^* - i^*) + \mu]$, where s^* and i^* are the equilibrium values for the susceptibles and infectives in the deterministic counterpart of the SIRS model (see

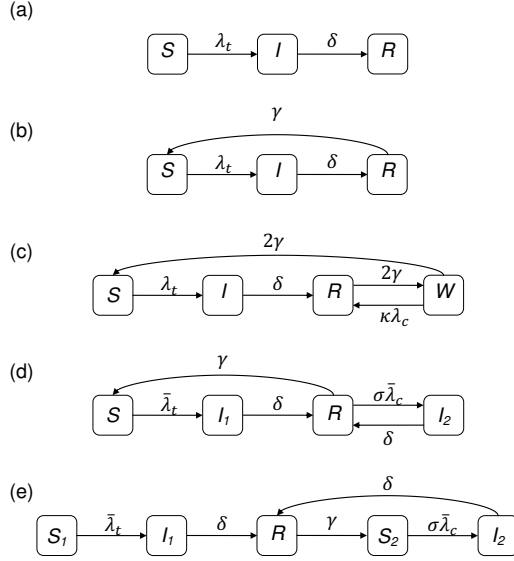


FIG. 1: The diagrams of five compartmental models for pertussis. The models (a) and (b) are the seasonally forced SIR and SIRS models, respectively, while the models (c), (d) and (e) are extensions of the SIR(S) paradigm. Model (c) allows for boosting of immunity proportional to, and potentially greater than, the force of infection, while model (d) allows for reinfection of recovered individuals. Model (e) accounts for a loss of infection-derived immunity and subsequent reinfection. In all diagrams, the transitions corresponding to the birth and death of individuals are not shown for simplicity. The meaning of the symbols associated with each transition is defined in the text.

the Supplementary Material for details on the deterministic SIRS model). Although there is no direct correspondence between primary infections and age groups in the model, it is reasonable to admit that a fraction of approximately $\gamma(1 - s^* - i^*)/[\gamma(1 - s^* - i^*) + \mu]$ of the infectives are not school children, and that β_1 should be reduced proportionally in this version of the model.

3. SIRWS model

Model (c) is an SIRS-type model allowing for immune boosting of recovered individuals upon reexposure to infectious individuals. In this model, infectives I recover at rate δ and

susceptibles S get infected at rate λ_t as in the SIR model. However, in addition to the S and I classes, there are two classes of recovered individuals denoted by R and W . The immunity of the former is not permanent and they move to the waning class W at a constant rate 2γ . The individuals in class W undergo two possible transitions: further immunity loss at rate 2γ to become susceptible S , or immunity boosting upon contact with infectious individuals to return to the recovered class R at a rate $\kappa\lambda_c = \kappa\beta_0 I/N$, where κ is the immunity boosting coefficient. We call this scheme the immune boosting model and denote it by SIRWS.

An age-structured version of this model with vaccination has been used to explain the recent reemergence of pertussis cases despite high vaccine coverage in Massachusetts, and also the shifts in total and age-specific incidences before and after mass vaccination [11].

4. *SIRIS model*

Model (d) proposed in [45] sets a scenario based on the SIRS model with a moderate rate γ of immunity loss where recovered individuals are immune to severe disease but susceptible with reduced susceptibility to mild forms of the disease. The classes of individuals infected with severe and mild infections are denoted by I_1 and I_2 , respectively. Recovery from both forms of the disease takes place at the same rate δ . Infectiousness of mild infections is reduced by a factor $\eta \in [0, 1]$ and susceptibility of recovered individuals to mild infections is also reduced by a factor $\sigma \in [0, 1]$ with respect to the susceptible. Moreover, since mild infections typically occur in adults that are not affected by seasonal forcing the force of infection is therefore taken to be $\bar{\lambda}_t = (\beta(t)I_1 + \beta_0\eta I_2)/N$ for susceptible individuals S and $\bar{\lambda}_c = \beta_0(I_1 + \eta I_2)/N$ for recovered individuals R . We call this scheme the reinfection model and denote it by SIRIS.

The main feature of this model is that it exhibits a reinfection threshold [46], that is, a value of infectiousness above which disease incidence rises by one or more orders of magnitude, due to high incidence levels of mild infections.

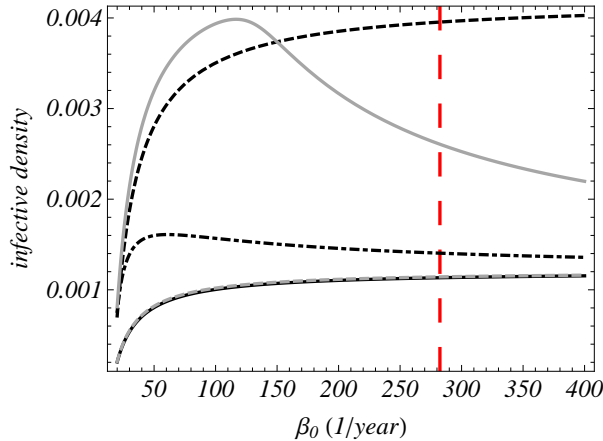


FIG. 2: (Color online) Infective density in the equilibrium of the unforced deterministic versions of the models, as a function of β_0 . The line stands for the I/N in the SIR (solid black), SIRS (dashed black) and SIRWS (dot-dashed black), and for the I_1/N in the SIRIS (solid gray) and SIRSI (dashed gray) model. The range of $\beta_0 = R_0(\delta + \mu)$ in the plot corresponds to $R_0 \in [1.2, 24]$, $\mu = 0.02 \text{ year}^{-1}$ and $\delta = 16.59 \text{ year}^{-1}$. Here R_0 is the so-called basic reproductive ratio of a disease defined as the average number of secondary cases generated by one infected individual in a fully susceptible population during one infectious period [47]. The red long-dashed vertical line indicates the value of β_0 for which $R_0 = 17$. Parameters: $\gamma = 1/20 \text{ year}^{-1}$ (SIRS model); $\gamma = 1/10 \text{ year}^{-1}$ (SIRWS model, [11]); $\gamma = 1/20 \text{ year}^{-1}$, $\eta = 0.5$, and $\sigma = 0.25$ (SIRIS model, [45]); $\gamma = 1/20 \text{ year}^{-1}$, $\eta = 0.1$, and $\sigma = 0.3$ (SIRSI model).

5. SIRSI model

Finally, model (e) proposed in [42] assumes an immune response that is a combination of (b) and (d), in the sense that recovered individuals are fully immune to the disease, but they lose this immunity at a certain rate γ to become susceptible to repeat infections, although with reduced susceptibility. The two classes of susceptible individuals are denoted by S_1 for the naive susceptibles and S_2 for the susceptibles generated by immunity waning, and $\sigma \in [0, 1]$ is the reduced susceptibility factor for repeat infections. The classes of individuals infected with first and repeat infections are denoted by I_1 and I_2 , respectively.

Recovery from both classes takes place at the same rate δ . The class of repeatedly infected individuals contributes with reduced infectiousness to the pool of infectives responsible for disease transmission, and $\eta \in [0, 1]$ is the reduced infectiousness factor. Repeat infections play a similar role in this model to that of mild infections in the SIRIS model, and the force of infection is taken to be $\bar{\lambda}_t = (\beta(t)I_1 + \beta_0\eta I_2)/N$ for S_1 and $\bar{\lambda}_c = \beta_0(I_1 + \eta I_2)/N$ for S_2 , because repeat infections typically occur in adults whose contacts are not subject to school term forcing. We call this scheme the repeat infection model and denote it by SIRSI.

We finish the description of the models by pointing out that, for a fixed β_0 , the unforced ($\beta_1 = 0$) deterministic counterparts of the five stochastic models introduced in this section have different densities of infectives in equilibrium. In Figure 2 we plot these equilibrium densities as a function of β_0 . The values of the remaining parameters will be justified later. For $0 < \beta_1 \lesssim 0.1$, the density of infectives in the deterministic versions of the five models oscillates with the period 1 year around the equilibrium value of the corresponding unforced equations (see the Supplementary Material). Note that the SIRWS model may have also limit cycles as stable attractors for some parameter values. This is, however, not the case for the parameter values that we will use in our analysis (β_0 fixed at the dashed vertical line in Fig. 2).

B. Data records

In this paper, we consider the historical data records for pre-vaccination pertussis incidence in Greater London in the period 1946-1957 (Figure 3, the left panel) and in Ontario in the period 1914-1943 (Figure 4, the left panels). The time series correspond to weekly data, in the case of London, and monthly data in the case of Ontario. Both raw and detrended (but not rescaled) data are shown for Ontario, where significant changes in population size and reporting efficiency are apparent during most of that period. In order to analyze the populations involved in these two data records, we shall consider only the undetrended data for Ontario corresponding to the last 8 years of the 29 years period. The ratio of the populations is close to 8/3.5, according to demographic data that set the population of Greater

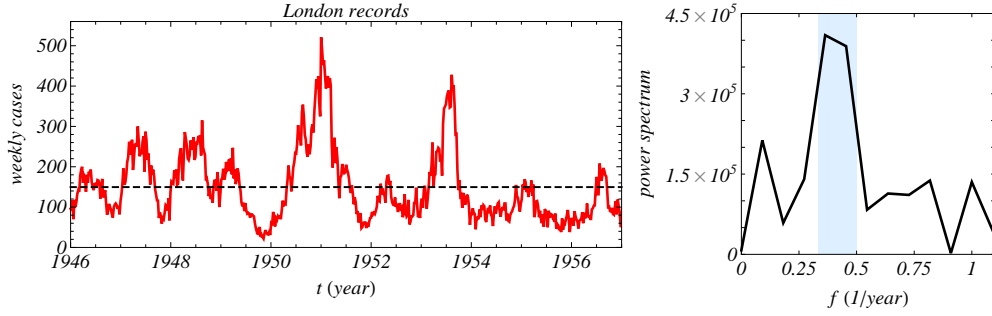


FIG. 3: (Color online) Left: new weekly cases of pertussis in (Greater) London before vaccination. The dashed horizontal line is the average number of weekly cases. Right: spectrum of the time series.

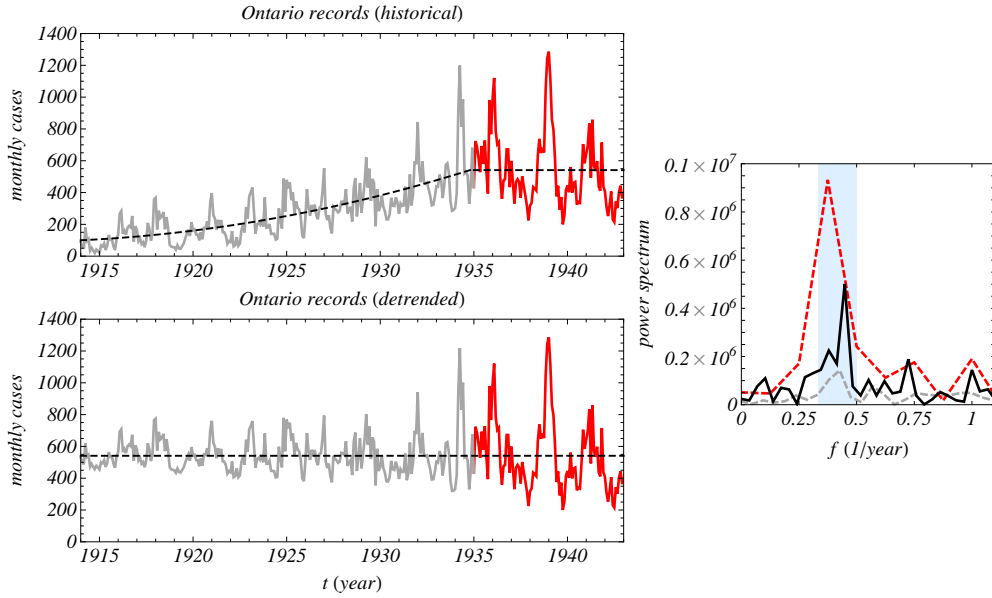


FIG. 4: (Color online) Left: new monthly cases of pertussis in the Canadian province Ontario before vaccination (upper panel) and the detrended time series (lower panel). The dashed horizontal line in the lower panel is the average number of monthly cases. Right: the solid black line is the spectrum of the full time series shown in the lower left panel, the red (black) dashed and the gray dashed lines are the spectra calculated from the detrended and undetrended partial time series shown in the same color.

London close to 8 million and that of Ontario close to 3.5 million in the period under consideration. However, the average recorded rate of new cases in a month interval, which is similar for the two data sets, points to a ratio of effective populations close to 1. Differences in surveillance coverage and/or in reporting efficiency could explain this. For London, levels of pertussis reporting efficiency in the range 5%-25% have been acknowledged in the literature [48]. The fact that the effective population for Ontario is approximately of the same size indicates that a higher reporting efficiency compensates for the smaller population.

It is known from the case notification data from England and Wales and other locations that the inter-epidemic periods for pertussis in the pre-vaccination era show significant multiannual structure. The multiannual periods lie in the range of 2-3 years and additionally annual outbreaks can be observed [18, 42, 49]. The power spectra computed from the data confirm these observations (see the right panels in Fig.3 and in Fig. 4). In the spectra plots, the shaded region marks the range of frequencies, $f \in [1/3, 1/2]$ year⁻¹, corresponding to the interepidemic periods $1/f \in [2, 3]$ years. Because of limited length and resolution in time, the spectra have a short range and a low resolution in frequency, however this affects mostly the annual peak. The widths of the multiannual peaks are comparable with each other. For Ontario, the power spectra of the full time series and of the detrended and undetrended partial data sets show the same dominant frequency components. In what follows, we shall consider only the power spectrum of the undetrended data.

C. Parameter values

The values of the demographic and epidemiological parameters that are well established in independent data sources are kept fixed (see, for example, [18, 47]). These are the birth/death rate μ (or the average lifespan $1/\mu$), the rate of recovery from infection δ (or average infectious period $1/\delta$) and the average contact rate β_0 . The value of the latter corresponds to the value of the basic reproductive ratio $R_0 = \beta_0/(\delta + \mu)$ reported in the literature for the two data sets considered in this study [18].

For the remaining parameters we either use the estimates found in the literature for

Epidemiological meaning	Notation	Value
<i>Per capita</i> birth/death rate	μ	0.02 year ⁻¹
Average lifespan	$1/\mu$	50 years
Rate of recovery from infection	δ	16.59 year ⁻¹
Average infectious period	$1/\delta$	22 days
Basic reproductive ratio	R_0	17
Average contact rate	β_0	282.39 year ⁻¹
Amplitude of seasonal forcing	β_1	[0, 0.1] year ⁻¹
Rate of loss of naturally acquired immunity	γ	[1/40, 1/10] year ⁻¹
Average infection-derived immunity period	$1/\gamma$	[10, 40] years
Relative infectiousness of repeat to primary (SIRSI) or mild to severe infections (SIRIS)	η	[0, 1]
Relative susceptibility of repeat to primary (SIRSI) or mild to severe infections (SIRIS)	σ	[0, 1]
Boosting coefficient	κ	20

TABLE I: The epidemiological description of the parameters and the range of their values for pertussis.

a particular model or explore an appropriate range of possible values if such estimates are absent. For example, the accepted range for the duration of naturally acquired immunity for pertussis is 7 to 20 years [50]. For the SIRS model, we take $1/\gamma$ equal 20 to 40 years. On one hand, the large upper limit allows for a comparison with the SIR model. On the other hand, as we shall see, taking $1/\gamma$ smaller than 20 years would make the prediction of the model worse. For the SIRIS model, we take $1/\gamma = 20$ years [45] and the relative infectiousness and relative susceptibility of mild infections $\eta, \sigma \in [0, 1]$. The prediction of this model for other values of $1/\gamma$ can still be done using the SIRS model as one of the limiting cases of the SIRIS model. For the SIRWS model, we take the value of the boosting coefficient $\kappa = 20$

and $1/\gamma = 10$ years considered in [11] and in addition we study the behavior of the model for $1/\gamma = 40$ years. For the SIRSI model, we set $1/\gamma = 20$ years and the relative infectiousness and relative susceptibility of repeat to primary infections $\eta, \sigma \in [0, 1]$ [42]. We discuss in the Supplementary Material the behavior of this model for other values of the duration of immunity.

For practical purposes we use only three values of the amplitude of seasonal forcing $\beta_1 = 0, 0.05, 0.1$. We will however discuss the predictions of the models for higher values of β_1 whenever necessary. The summary of the parameter values is given in Table I.

D. Stochastic simulations

To study the behavior of the five candidates for the description of pre-vaccination pertussis we use stochastic simulations of the processes described in Fig. 1. The simulations are based on a modification of Gillespie's algorithm [51] which accounts for the explicit time dependence in the contact rate [52],[53]. In Sections III A-III D, each simulation run starts from a random initial condition and the prevalence of the disease is recorded with a time step of 0.05 year for 450 years after 50 years of transient. From each simulation run the power spectrum of the prevalence time series is computed with the use of the discrete Fourier transform. The final spectra are averages of 10^3 simulations. The population size, N , used in the simulations in Sections III A-III D is 5×10^5 .

III. RESULTS

We investigate the dynamics of the stochastic seasonally forced SIR, SIRS, SIRWS, SIRIS and SIRSI models by comparing the power spectra of long time series of the five models in the relevant parameter ranges. In all cases, the spectra correspond to the fluctuations around the equilibrium of the unforced deterministic versions of each model ($\beta_1 = 0$) or around the associated period one year stable attractor ($\beta_1 > 0$). Numerical and simulational results for the parameter ranges we have explored never showed evidence of other attractors. A direct

quantitative comparison of these power spectra with the spectra shown in Fig. 3 and Fig. 4 based on the amplitude of the multiannual peaks and their precise location is undermined by the low resolution in frequency and poor statistics of the two data sets, which correspond to much shorter periods than the ones that can be used in the numerical simulations. That is why our first criterion in making the comparison between the models' predictions and the spectra computed from the data will be the position of the multiannual peak. In order to be able to explain historical data records of pertussis incidence a model's spectrum should have the multiannual peak located in the range of frequencies, $f \in [1/3, 1/2]$ year⁻¹ (see Fig. 3 and Fig. 4). This region is the shaded region shown in all spectra plots throughout the paper.

As pointed out before, in Sections III A-III D we use a typical population size $N = 5 \times 10^5$ in all models and compute spectra from the prevalence time series. Changing population size and/or computing the incidence in a given interval instead of the prevalence of the disease may change somewhat the amplitude of the multiannual and annual peaks but does not influence their position.

A. SIRS model

In the SIRS model, the rate of immunity waning γ is a free parameter. In the case of the lifelong immunity, $\gamma = 0$, the SIRS model reduces to the SIR model which we consider later. Figure 5 shows the model's power spectrum as a function of frequency for different values of the forcing amplitude β_1 and two typical values of γ . The power spectra computed from the stochastic simulations exhibit two types of peaks: a well defined dominant annual peak due to the deterministic annual limit cycle and a subdominant broad multiannual stochastic peak with the shape and the main frequency similar to that of the unforced case. As seen from the comparison of the middle and right panels in Fig. 5, for fixed γ the increase in β_1 results in a more enhanced annual peak which means that the contribution of annual epidemics in the time series increases as β_1 increases. The multiannual stochastic peak reflects the presence of noisy oscillations in the incidence time series with that dominant

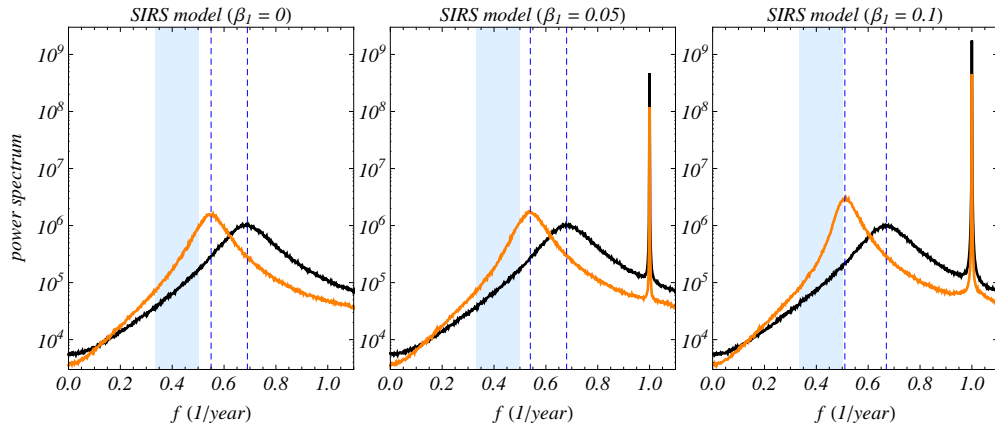


FIG. 5: (Color online) The average power spectra from simulations of the SIRS model for different amplitudes of seasonal forcing, β_1 , and two values of the immunity waning rate, γ . Parameters: $1/\gamma = 20$ years (black), 40 years [orange (gray)]. The multiannual peaks of the spectra computed from the London and Ontario data sets are located in the shaded region. Henceforth, all simulation spectrum plots will be shown in lin-log scale and the dashed lines will indicate the dominant frequency of the stochastic multiannual peaks of the simulations.

frequency. The mechanisms by which internal noise excites these resonant fluctuations has been treated in several papers [27, 28, 31, 32, 43]. They can be described analytically using van Kampen’s expansion of the master equation of the underlying stochastic process around the attractor of the deterministic system [54]. We point out that in this study the dominant frequency of the main stochastic peak in the seasonally forced models can be computed from the unforced model whose analysis is easier (see Supplementary Material for more information on the analytical computation of the power spectra).

In the unforced SIRS model, $\beta_1 = 0$, the spectrum does have a pronounced stochastic peak. However, it is situated outside the region of interest both for $\gamma = 1/40 \text{ year}^{-1}$ and for $\gamma = 1/20 \text{ year}^{-1}$. For fixed γ and increasing β_1 , the frequency of the stochastic peak is slightly shifted towards the target region but it remains outside it even for large values of γ and, at the same time, the power associated with the annual peak becomes very large. Note that if β_1 is decreased to take into account that non primary infections should not be

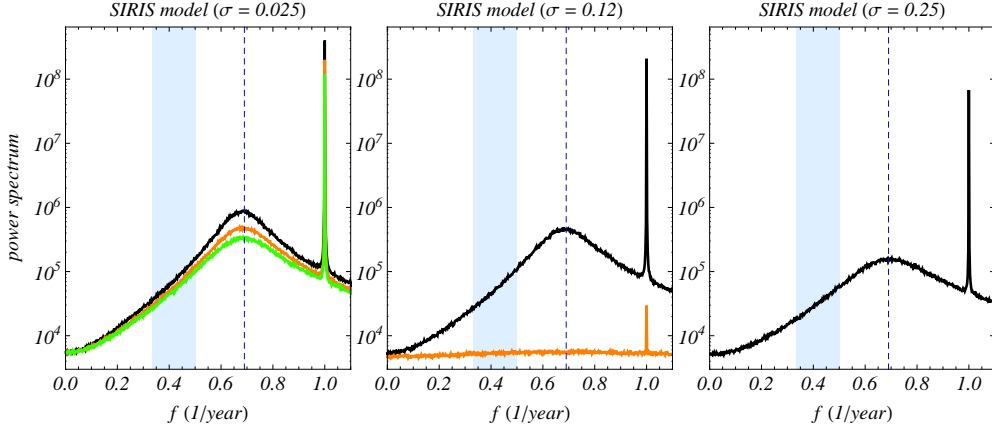


FIG. 6: (Color online) The average power spectra from simulations of the SIRIS model for $\beta_1 = 0.05$, $\gamma = 1/20 \text{ year}^{-1}$ and different values of the relative infectiousness, η , and relative susceptibility, σ , of mild to severe infections. Parameters: $\eta = 0.1$ (black), 0.5 [orange (dark gray)] and 0.75 [green (light gray)]. The values of η and σ were chosen from $(0,1)$ so as to guarantee that the equilibrium incidence in the unforced deterministic SIRIS model is of the same order of magnitude as in the SIR(S) models. The multiannual peaks of the spectra computed from the London and Ontario data sets are located in the shaded region. The dashed lines indicate the dominant frequency of the multiannual peaks of the simulations.

subject to seasonal forcing in this model the dominant frequency of the stochastic peak is moved even further away from the shaded region.

B. SIRIS model

Next we analyze the power spectra from simulations of the SIRIS model. This model has three free parameters apart from the amplitude of seasonal forcing β_1 : the rate of immunity loss γ , and the relative infectiousness η and relative susceptibility σ . For the limiting case of $\eta = 0$ and $\sigma = 0$ the model reduces to the SIRS model whose multiannual peaks are located outside the shaded region. The model's behavior is, however, well understood if we vary only η and σ . The results are shown in Fig. 6 for fixed $\beta_1 = 0.05$ and $\gamma = 1/20$

year⁻¹. The spectrum for small values of η and σ is reminiscent of the SIRS model. A comparison of the spectra in all panels of Fig. 6 shows that the stochastic and deterministic peaks are the highest for the smallest values of both η and σ . This is because it is easier to generate incidence oscillations in this parameter range. The increase in the values of η and σ results in a flattening of the spectrum occurring through a gradual disappearance of, first, stochastic and, then, deterministic peaks. Moreover, the study of the dependence of the power spectrum on the amplitude of seasonal forcing β_1 does not change this picture. For example, for the smallest values of η and σ used in Fig. 6 we observe that the position and the shape of the stochastic peaks agree perfectly for $\beta_1 \in [0, 0.1]$ and that they are always outside of the region of interest (this result is given in the Supplementary Material). The parameter region with higher values of η and σ is even less interesting because of the flattening of the spectrum. Thus for all relevant ranges of η , σ and β_1 the stochastic multiannual peak in this model is situated outside the region of interest except when it approaches the limit of the SIR model whose behavior we will discuss later.

C. SIRWS model

The power spectra computed from simulations of the SIRWS model for boosting coefficient $\kappa = 20$ and different values of γ and β_1 are shown in Fig. 7. In the absence of seasonality, $\beta_1 = 0$, the spectra have a dominant multiannual peak situated in the target region for the whole range of $\gamma \in [1/40, 1/20]$ year⁻¹. When β_1 increases a deterministic annual peak appears in the spectrum while the dominant frequency of the multiannual peak stays unchanged. Similarly to the SIRS model, the higher the amplitude of seasonal forcing β_1 is the higher the annual peak is. However, unlike in that model, this phenomenon is accompanied by an overall complication of the structure of the spectrum for higher values of β_1 . For example, the power spectrum for $\gamma = 1/10$ year⁻¹ and $\beta_1 = 0.1$ (black line in the right panel of Fig. 7) has several secondary multiannual peaks, one of which is situated near but outside the shaded region. Thus, the SIRWS model predicts a rather broad range of frequencies corresponding to the stochastic fluctuations around the annual deterministic

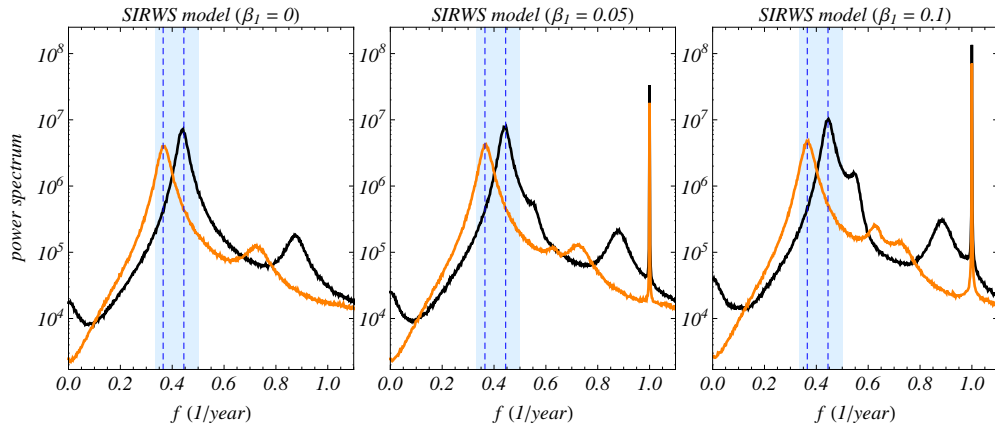


FIG. 7: (Color online) The average power spectra from simulations of the SIRWS model for different amplitudes of seasonal forcing, β_1 , and two values of the immunity waning rate, γ . Parameters: $1/\gamma = 10$ years (black) and 40 years [orange (gray)]. The immune boosting coefficient $\kappa = 20$ is all panels. The multiannual peaks of the spectra computed from the London and Ontario data sets are located in the shaded region. The dashed lines indicate the dominant frequency of the multiannual peaks of the simulations.

cycle.

D. SIR and SIRSI models

Finally, we compare the power spectra from simulations of the SIR and SIRSI models. Figure 8 shows the spectra for different values of $\beta_1 \in [0, 0.1]$. Similarly to the previous results, the simulation spectra of the SIR and SIRSI models have a high stochastic multiannual peak in addition to the annual peak due to the deterministic limit cycle. The amplitude of the deterministic peaks and therefore the power associated with them increase as β_1 increases while the stochastic peaks stay almost unchanged. The increase, however, is smaller in the SIRSI model than in the SIR model. This means that, notwithstanding the similarity of their simulation spectra, the contribution of annual epidemics is less in the former than in the latter, corresponding to a qualitative difference in the times series of the two models.

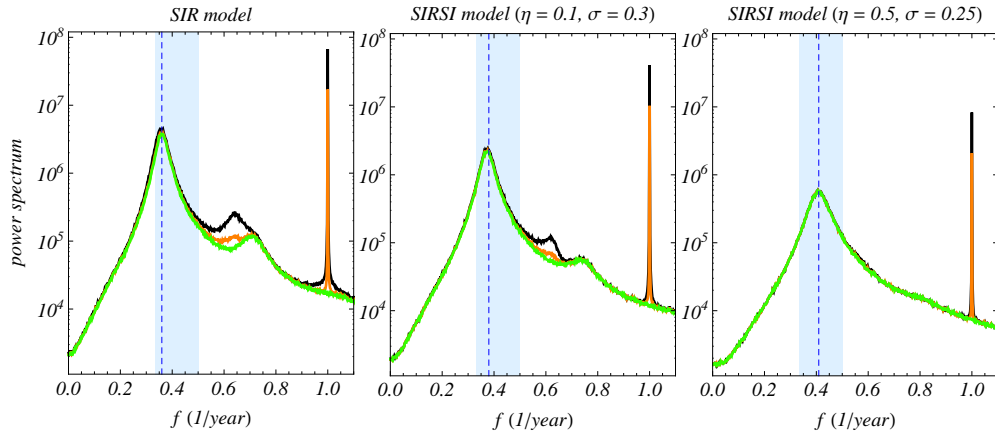


FIG. 8: (Color online) The power spectrum from simulations of the SIR and SIRSI models. Parameters: $\beta_1 = 0$ [green (light gray)], 0.05 [orange (dark gray)] and 0.1 (black), $1/\gamma = 20$ years (the SIRSI model). The values of the relative infectiousness η and the relative susceptibility σ of repeat to primary infections were chosen from a set of all possible values explored in the Supplementary Material. The multiannual peaks of the spectra computed from the London and Ontario data sets are located in the shaded region. The dashed lines indicate the dominant frequency of the multiannual peaks of the simulations.

For both models, the frequency and the shape of the dominant stochastic peak are largely independent of β_1 , and the peak's frequency lies in the shaded region. The dominant period of stochastic fluctuations in the SIR model is 2.73 years. In the SIRSI model, for fixed γ , we considered in the interval $(0, 1)$ nine equally spaced values and constructed a grid of 81 points in the (η, σ) space. As the position and the shape of the stochastic peak in this model is independent of β_1 we can calculate the stochastic peak's frequency from the unforced model (see Supplementary Material for more details). For example, for $\gamma = 1/20$ year $^{-1}$ used in Fig. 8, the number of spectra for the SIRSI model with the stochastic peak within the shaded region is 62 (for $1/\gamma \in [10, 40]$ years this number varies from 43 to 78). We thus conclude that the SIRSI model's spectrum illustrated in Fig. 8 is robust with respect to variation of all free parameters, and that it exhibits some degree of variability in the amplitude of the stochastic multiannual peak as parameters are varied within their accepted

ranges.

E. Comparison with real data

The results for the power spectra of stochastic simulations show that out of the five models under consideration only SIRWS, SIR and SIRSI have frequency values for the stochastic multiannual peak compatible with data for pre-vaccination pertussis. Here we compare the spectra of these three models with the spectra for London and Ontario data sets shown in Figs. 3 and 4.

As a first step towards achieving this we determine the population size N for each model. As discussed before both data sets have the similar average recorded rate of new cases in a month interval and thus correspond to a similar effective population. However, the deterministic counterparts of the models, and consequently the stochastic models too, predict different densities of infectives in the steady state. To resolve this, for each of the three models we make simulations with the same length and the same sampling time as those of the London or Ontario data sets and record the incidence of the disease in the sampling interval. The transient period in all simulations is taken to be 50 years and each simulation starts from a random initial condition. We calibrate the effective population size N for a given model by imposing that the incidence averaged over 10^3 different simulation runs is the same as the time averaged incidence in the corresponding data set, given by the dashed line in Fig. 3 and in Fig. 4. In Fig. 9 we show typical incidence time series for $\beta_1 = 0.05$ and the effective population size N for each of the three models from which individual power spectra are computed.

The second step is to determine for each model the level of seasonality that corresponds to the data set. We estimate the value of the amplitude of the seasonal forcing β_1 as the value for which the amplitude of the annual deterministic peak in the power spectrum of incidence times series averaged over 10^3 different simulation runs is equal to the amplitude of the annual peak in the spectrum computed from the data.

Using the values of N and of β_1 determined in this way, we produce from the stochastic

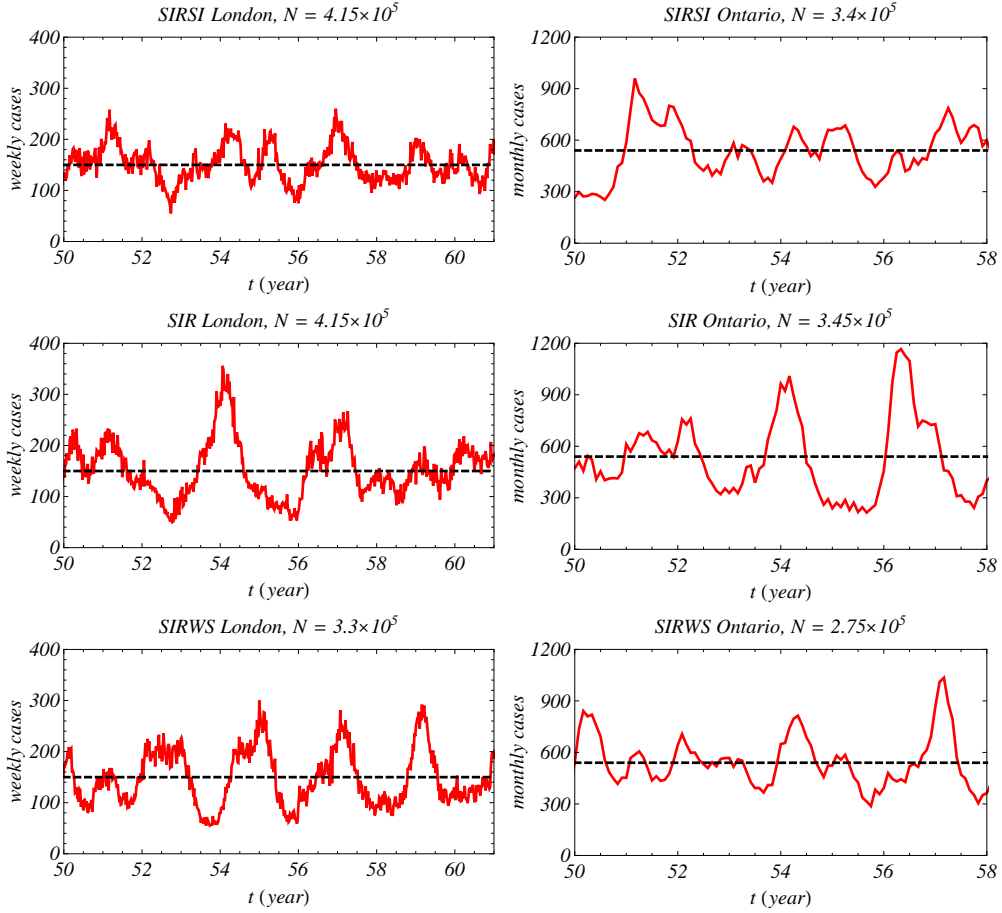


FIG. 9: (Color online) Incidence of the disease in a simulation of the SIRWS, SIR and SIRSI models. The horizontal dashed line is the average number of weekly (London) or monthly (Ontario) cases (compare these with the dashed lines in Fig. 3 and in Fig. 4). Parameters: $\beta_1 = 0.05$ (all plots); $\kappa = 20$, $1/\gamma = 10$ years (SIRWS model, the black line in the middle plot of Fig. 7); $1/\gamma = 20$ years, $\eta = 0.1$, $\sigma = 0.1$ (SIRSI model Ontario) and $\sigma = 0.3$ [SIRSI model London, the orange (dark gray) line in the middle plot of Fig. 8]. Note that the level of seasonal forcing β_1 does not change the average incidence.

models time series mimicking the London or Ontario data sets, and average their power spectra over 10^3 simulation runs. The power spectra from simulation [dashed red (black) lines] and the spectra computed from the data sets [black solid lines] are shown in Fig. 10.

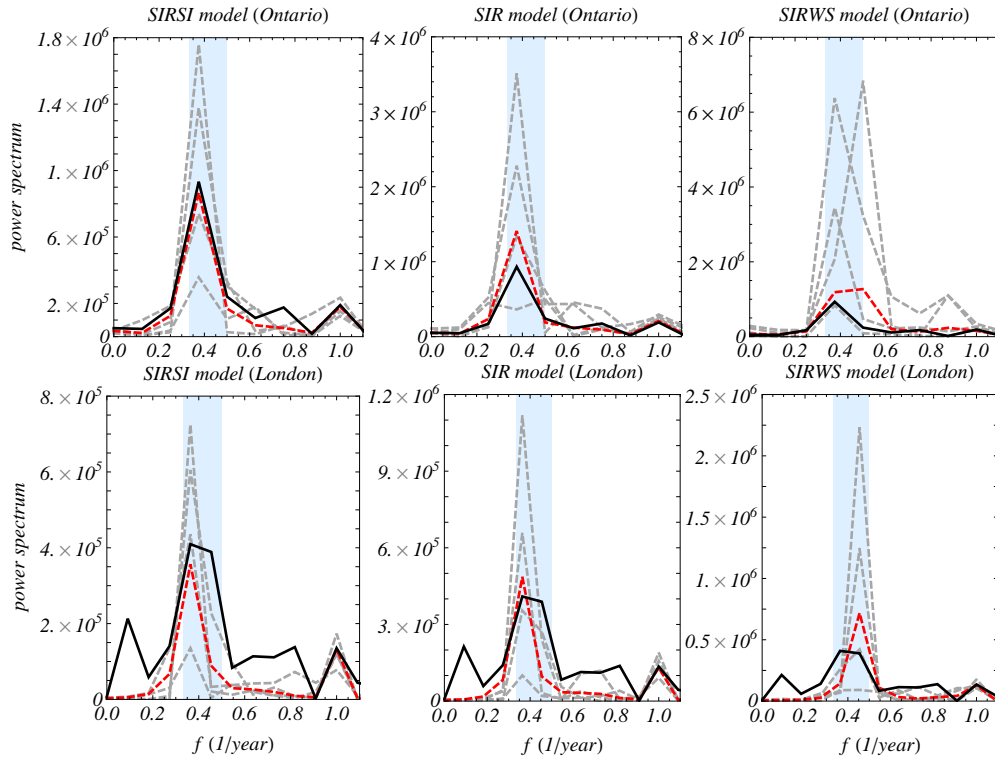


FIG. 10: (Color online) The solid black line is the power spectrum of the London or Ontario data sets as indicated in each panel. The dashed red (black) line is the average power spectrum of the incidence time series computed from 10^3 simulation runs with the same length and the same sampling time as those of the London or Ontario data sets. The dashed gray lines are four typical power spectra computed from an individual simulation. Parameters: $\beta_1 = 0.06$ (SIRSI Ontario), $\beta_1 = 0.07$ (SIRSI London), $\beta_1 = 0.05$ (SIR Ontario), $\beta_1 = 0.06$ (SIR London), $\beta_1 = 0.03$ (SIRWS Ontario), $\beta_1 = 0.05$ (SIRWS London). The remaining parameter values are as in Fig. 9.

For the SIRSI (respectively, SIR, SIRWS) model these average power spectra have stochastic multiannual peaks with similar (respectively, similar, larger) amplitude than those of the data sets power spectra.

The results of Fig. 10 suggest that the SIRSI model is the one that best reproduces the stochastic properties of both data sets. However, as shown by the four examples plotted in the figure for each case (dashed gray lines), the poor statistics of the short term samplings

translates into a considerable variability in the power spectra computed from each time series. The two historical data records considered here illustrate the principle that the incidence power spectra can be used to discriminate the three variants of the model, but a final conclusion on their performance would require the analysis of longer time series.

IV. DISCUSSION AND CONCLUSIONS

Different assumptions about disease and vaccine induced immunity have been proposed in the recent literature to model the dynamics of pertussis in the presence of mass vaccination. Our motivation has been to study separately the influence of disease acquired immunity only, in order to reduce the number of free parameters, and to consider explicitly the stochastic properties of the incidence time series as part of the model's output, in order to look for further constraints.

We have used the basic SIR model and four variants that reflect different immune responses. We characterized the dynamic patterns of each of these five models through the average power spectra of an ensemble of long term prevalence time series obtained from stochastic simulations. We have found that the power spectra of the five alternative models show quantitative and even qualitative differences. One of them (SIRS) fails to reproduce a stochastic peak in the frequency range found in real data for pertussis, and another one (SIRIS) is too stiff to produce stochastic fluctuations with the observed amplitudes.

Assessing the other three models (SIR, SIRWS and SIRSI) requires a quantitative comparison of the simulated power spectra with real data, for which purpose the effective population size and the forcing amplitude of each data record must be determined. We illustrated this procedure by considering two publicly available historical data records for pre-vaccination pertussis incidence. Based on these relatively short time series, we found that the SIRSI model seems to reproduce the main aspects of the phenomenology of the disease in a broad parameter range, reproducing the multiannual interepidemic periods and the amplitude of fluctuations found in the data, while the other two models tend to produce larger stochastic fluctuations.

Considerations about the recovery profile and its influence on the model's behavior concur in favoring models such as SIRSI, with a much flatter spectrum than its alternatives. Here we have followed the common approach of taking recovery as a constant rate stochastic process, instead of more realistic unimodal recovery profiles that have been proposed and studied in the literature [30, 55]. For unforced models, it is known [30] that the effect of this change is twofold, on one hand a small displacement of the main stochastic peak towards higher frequencies, and on the other an enhancement of the fluctuations. We have checked (results not shown) that this holds too for the SIRSI and SIRWS models in the parameter region explored in the previous section when we change from an exponentially distributed recovery profile to a unimodal gamma distributed recovery profile with the same average. Therefore, under more realistic recovery profiles, the output of the SIR and SIRWS models would be further away from the target power spectra.

However, the short length of the time series used in our illustrative study prevents any definite conclusion about the performance of the SIR and SIRWS alternatives. Indeed, the ensemble of the power spectra obtained from simulated time series of this length exhibits enough variability to accommodate the two samples of real data. An extension of this analysis to a larger set of data could help to further elucidate the dynamics of disease acquired immunity, setting a solid ground for more complex models to deal with vaccine acquired immunity.

V. ACKNOWLEDGEMENTS

The authors thank Gabriela Gomes for helpful discussions. Financial support from the Portuguese Foundation for Science and Technology (FCT) under Contract No. POCTI/ISFL/2/261 is gratefully acknowledged. The first author (G.R.) was also supported by FCT under Grants No. SFRH/BD/32164/2006 and No. SFRH/BPD/ 69137/2010, and by Calouste Gulbenkian Foundation under its Program "Stimulus for Research". This research was also partially supported by the National Science Foundation under Grant No. NSF PHY05-51164. The data used in this paper are available online from the International

- [1] Trottier, H., Philippe, P. & Roy, R. 2006 Stochastic modeling of empirical time series of childhood infectious diseases data before and after mass vaccination. *Emerg. Themes Epidemiol.* **3**. (doi:10.1186/1742-7622-3-9)
- [2] <http://www.math.mcmaster.ca/~bolker/measdata/>.
- [3] Yorke, J. A. & London, W. P. 1973 Recurrent outbreaks of measles, chickenpox and mumps: II. Systematic differences in contact rates and stochastic effects. *Am. J. Epidemiol.* **98**, 469–482.
- [4] Wallinga, J., Lévy-Bruhl, D., Gay, N. J. & Wachmann, C. H. 2001 Estimation of measles reproduction ratios and prospects for elimination of measles by vaccination in some Western European countries. *Epidemiol. Infect.* **127**, 281–295.
- [5] Broutin, H., Guégan, J. F., Elguero, E., Simondon, F. & Cazelles, B. 2005 Large-scale comparative analysis of pertussis population dynamics: periodicity, synchrony, and impact of vaccination. *Am. J. Epidemiol.* **161**, 1159–1167.
- [6] Broutin, H., Mantilla-Beniers, N. B., Simondon, F., Aaby, P., Grenfell, B. T., Guégan, J. F. & Rohani, P. 2005 Epidemiological impact of vaccination on the dynamics of two childhood diseases in rural Senegal. *Microbes Infect.* **7**, 593–599.
- [7] Centers for Disease Control and Prevention. 2002 Pertussis – United States, 1997-2000. *MMWR* **51**, 73-76.
- [8] Skowronski, D. M., De Serres, G., MacDonald, D., Wu, W., Shaw, C., Macnabb, J., Champagne, S., Patrick, D. M. & Halperin, S. A. 2002 The changing age and seasonal profile of pertussis in Canada. *J. Infect. Dis.* **185**, 1448–1453.
- [9] de Melker, H. E., Schellekens, J. F., Neppelenbroek, S. E., Mooi, F. R., Rümke, H. C. & Conyn-van Spaendonck, M. A. 2000 Reemergence of pertussis in the highly vaccinated population of the Netherlands: observations on surveillance data. *Emerg. Infect. Dis.* **6**, 348–357.
- [10] Crowcroft, N. S. & Pebody, R. G. 2006 Recent developments in pertussis. *Lancet* **367**, 1926–

1936.

- [11] Lavinea, J. S., King, A. A., & Bjørnstad, O. N. 2011 Natural immune boosting in pertussis dynamics and the potential for long-term vaccine failure. *Proc. Natl. Acad. Sci. U.S.A.* (doi:10.1073/pnas.1014394108)
- [12] Soper, H. 1929 The interpretation of periodicity in disease prevalence. *J. R. Stat. Soc.* **92**, 34-73.
- [13] London, W. P. & Yorke, J. A. 1973 Recurrent outbreaks of measles, chickenpox and mumps. I. Seasonal variation in contact rates. *Am. J. Epidemiol.* **98**, 453-468.
- [14] Fine, P. E. & Clarkson, J. A. 1982 Measles in England and Wales-I: An analysis of factors underlying seasonal patterns. *Int. J. Epidemiol.* **11**, 5-14.
- [15] Fine, P. E. & Clarkson, J. A. 1986 Seasonal influences on pertussis. *Int. J. Epidemiol.* **15**, 237-247.
- [16] Grenfell, B. T., Bjørnstad, O. N. & Kappey, J. 2001 Travelling waves and spatial hierarchies in measles epidemics. *Nature* **414**, 716-723.
- [17] Earn, D. J. D., Rohani, P., Bolker, B. M. & Grenfell, B. T. 2000 A simple model for complex dynamical transitions in epidemics. *Science* **287**, 667-670.
- [18] Bauch, C. T. & Earn, D. J. D. 2003 Transients and attractors in epidemics. *Proc. R. Soc. Lond. B* **270**, 1573-1578.
- [19] Keeling, M. J., Rohani, P. & Grenfell, B. T. 2001 Seasonally forced disease dynamics explored as switching between attractors. *Physica D* **148**, 317-335.
- [20] Wearing, H. J., Rohani, P. & Keeling, M. J. 2005 Appropriate modeling of infectious diseases. *PLoS Med.* **2**, e239. (doi:10.1371/journal.pmed.0020239)
- [21] Simões, M., Telo da Gama, M. M. & Nunes, A. 2008 Stochastic fluctuations in epidemics on networks. *J. R. Soc., Interface* **5**, 555-566.
- [22] Edmunds, W. J., Kafatos, G., Wallinga, J. & Mossong, J. R. 2006 Mixing patterns and the spread of close-contact infectious diseases. *Emerg. Themes Epidemiol.* **3**. (doi:10.1186/1742-7622-3-10)
- [23] Read, J. M., Eames, K. T. & Edmunds, W. J. 2008 Dynamic social networks and the impli-

- cations for the spread of infectious disease. *J. R. Soc., Interface* **5**, 1001–1007.
- [24] Hethcote, H. W. 1997 An age-structured model for pertussis transmission. *Math. Biosci.* **145**, 89–136.
- [25] Allen, L. J. & Driessche, P. 2006 Stochastic epidemic models with a backward bifurcation. *Math. Biosci. Eng.* **3**, 445–458.
- [26] Keeling, M. J. & Eames, K. T. 2005 Networks and epidemic models. *J. R. Soc., Interface* **2**, 295–307.
- [27] Alonso, D., McKane, A. J. & Pascual, M. 2007 Stochastic amplification in epidemics. *J. R. Soc., Interface* **4**, 575–582.
- [28] Rozhnova, G. & Nunes, A. 2009 Fluctuations and oscillations in a simple epidemic model. *Phys. Rev. E* **79**, 041922.
- [29] Volz, E. & Meyers, L. A. 2009 Epidemic thresholds in dynamic contact networks. *J. R. Soc., Interface* **6**, 233–241.
- [30] Black, A. J., McKane, A. J., Nunes, A. & Parisi, A. 2009 Stochastic fluctuations in the susceptible-infective-recovered model with distributed infectious periods. *Phys. Rev. E* **80**, 021922.
- [31] Black, A. J. & McKane, A. J. 2010 Stochastic amplification in an epidemic model with seasonal forcing. *J. Theor. Biol.* **267**, 85–94.
- [32] Rozhnova, G. & Nunes, A. 2010 Stochastic effects in a seasonally forced epidemic model. *Phys. Rev. E* **82**, 041906.
- [33] Metcalf, C. J., Bjørnstad, O. N., Grenfell, B. T. & Andreasen, V. 2009 Seasonality and comparative dynamics of six childhood infections in pre-vaccination Copenhagen. *Proc. R. Soc. B* **276**, 4111–4118.
- [34] Grassly, N. C. & Fraser, C. 2006 Seasonal infectious disease epidemiology. *Proc. R. Soc. B* **273**, 2541–2550.
- [35] Meyers, L. A., Pourbohloul, B., Newman, M. E., Skowronski, D. M. & Brunham, R. C. 2005 Network theory and SARS: predicting outbreak diversity. *J. Theor. Biol.* **232**, 71–81.
- [36] Eubank, S., Guclu, H., Kumar, V. S., Marathe, M. V., Srinivasan, A., Toroczkai, Z. & Wang,

- N. 2004 Modelling disease outbreaks in realistic urban social networks. *Nature* **429**, 180–184.
- [37] Broutin, H., Viboud, C., Grenfell, B. T., Miller, M. A. & Rohani, P. 2010 Impact of vaccination and birth rate on the epidemiology of pertussis: a comparative study in 64 countries. *Proc. R. Soc. B* **277**, 3239–3245.
- [38] Rohani, P., Keeling, M. J. & Grenfell, B. T. 2002 The interplay between determinism and stochasticity in childhood diseases. *Am. Nat.* **159**, 469–481.
- [39] Nguyen, H. T. & Rohani, P. 2008 Noise, nonlinearity and seasonality: the epidemics of whooping cough revisited. *J. R. Soc., Interface* **5**, 403–413.
- [40] Ferrari, M. J., Grais, R. F., Bharti, N., Conlan, A. J., Bjørnstad, O. N., Wolfson, L. J., Guerin, P. J., Djibo, A. & Grenfell, B. T. 2008 The dynamics of measles in sub-Saharan Africa. *Nature* **451**, 679–684.
- [41] Mantilla-Beniers, N. B., Bjørnstad, O. N., Grenfell, B. T. & Rohani, P. 2010 Decreasing stochasticity through enhanced seasonality in measles epidemics. *J. R. Soc., Interface* **7**, 727–739.
- [42] Wearing, H. J. & Rohani, P. 2009 Estimating the duration of pertussis immunity using epidemiological signatures. *PLoS Pathog.* **5**, e1000647. (doi:10.1371/journal.ppat.1000647)
- [43] Black, A. J. & McKane, A. J. 2010 Stochasticity in staged models of epidemics: quantifying the dynamics of whooping cough. *J. R. Soc., Interface* **7**, 1219–1227.
- [44] Rohani, P., Zhong, X. & King, A. A. 2010 Contact network structure explains the changing epidemiology of pertussis. *Science* **330**, 982–985.
- [45] Aguas, R., Goncalves, G. & Gomes, M. G. 2006 Pertussis: increasing disease as a consequence of reducing transmission. *Lancet Infect. Dis.* **6**, 112–117.
- [46] Gomes, M. G., White, L. J. & Medley, G. F. 2004 Infection, reinfection, and vaccination under suboptimal immune protection: epidemiological perspectives. *J. Theor. Biol.* **228**, 539–549.
- [47] Anderson, R. A. & May, R. M. 1991 *Infectious Diseases of Humans*. Oxford, Oxford University Press.
- [48] Clarkson, J. A. & Fine, P. E. M. 1985 The efficiency of measles and pertussis notification in England and Wales. *Int. J. Epidemiol.* **14**, 153–168.

- [49] Rohani, P., Earn, D. J. D. & Grenfell, B. T. 1999 Opposite patterns of synchrony in sympatric disease metapopulations. *Science* **286**, 968–971.
- [50] Wendelboe, A. M., Van Rie, A., Salmaso, S. & Englund, J. A. 2005 Duration of immunity against pertussis after natural infection or vaccination. *Pediatr. Infect. Dis. J.* **24**, S58-S61.
- [51] Gillespie, D. T. 1976 A general method for numerically simulating the stochastic time evolution of coupled chemical reactions. *J. Comput. Phys.* **22**, 403–434.
- [52] Anderson, D. F. 2007 A modified next reaction method for simulating chemical systems with time dependent propensities and delays. *J. Chem. Phys.* **127**, 214107.
- [53] Lu, T., Volfson, D., Tsimring, L. & Hasty, J. 2004 Cellular growth and division in the Gillespie algorithm. *Syst. Biol.* **1**, 121–128.
- [54] van Kampen, N. G. 1992 *Stochastic processes in physics and chemistry*. Amsterdam, The Netherlands: Elsevier.
- [55] Lloyd, A. L. 2001 Destabilization of epidemic models with the inclusion of realistic distributions of infectious periods. *Proc. R. Soc. Lond. B* **268**, 985–993.

Modeling the long term dynamics of pre-vaccination pertussis

Supplementary Material

Ganna Rozhnova^{*1,2} and Ana Nunes¹

¹*Centro de Física da Matéria Condensada and Departamento de Física,
Faculdade de Ciências da Universidade de Lisboa,
P-1649-003 Lisboa Codex, Portugal*

²*Kavli Institute for Theoretical Physics, Kohn Hall,
University of California, Santa Barbara, CA 93106-4030*

arXiv:1104.5112v2 [q-bio.PE] 25 Feb 2012

* corresponding author
a_rozhnova@cii.fc.ul.pt

Supplementary Online Material Outline

- I. Deterministic counterparts of the SIR, SIRS, SIRIS, SIRWS and SIRSI models.
- II. SIRIS model for $\beta_1 \neq 0.05$.
- III. Analytical computation of the dominant frequency of the multiannual peak.

I. DETERMINISTIC COUNTERPARTS OF THE SIR, SIRS, SIRIS, SIRWS AND SIRSI MODELS.

In the infinite population limit, $N \rightarrow \infty$, the equations of the SIR model for the susceptible and infective densities are

$$\frac{ds}{dt} = \mu(1 - s) - \beta(t)si, \quad (1)$$

$$\frac{di}{dt} = \beta(t)si - (\delta + \mu)i, \quad (2)$$

where

$$\beta(t) = \beta_0(1 + \beta_1 \cos 2\pi t). \quad (3)$$

The density of recovered individuals is thus given by

$$r = 1 - s - i. \quad (4)$$

For $\beta_1 = 0$, seasonal forcing is absent and the system has a trivial ($i^* = 0$, $s^* = 1$) and a nontrivial fixed point. The latter can be expressed in terms of the basic reproductive ratio R_0 of a disease defined as the average number of secondary cases generated by one infected individual in a fully susceptible population during one infectious period:

$$i^* = \frac{\mu(R_0 - 1)}{\beta_0}, \quad s^* = \frac{1}{R_0}, \quad (5)$$

where

$$R_0 = \frac{\beta_0}{\delta + \mu}. \quad (6)$$

Stability analysis shows that the trivial equilibrium is stable if $R_0 < 1$ while the endemic equilibrium (5) is stable if $R_0 > 1$. This means that the critical value of R_0 given by Eq. (6) above which the disease is endemic is 1.

In the infinite population limit, the equations of the SIRS model are

$$\frac{ds}{dt} = \mu(1 - s) - \beta(t)si + \gamma r, \quad (7)$$

$$\frac{di}{dt} = \beta(t)si - (\delta + \mu)i, \quad (8)$$

where $\beta(t)$ and r are given by Eqs. (3) and (4), respectively. For $\beta_1 = 0$ the non trivial equilibrium values s^* and i^* of the model satisfy

$$i^* = \frac{(\gamma + \mu)(\delta + \mu)(R_0 - 1)}{\beta_0(\gamma + \delta + \mu)}, \quad s^* = \frac{1}{R_0}, \quad (9)$$

where R_0 is given by Eq. (6).

In the infinite population limit, the equations of the SIRWS model for the densities of individuals in the susceptible, infectious and waning classes are

$$\frac{ds}{dt} = \mu(1 - s) - \beta(t)si + 2\gamma w, \quad (10)$$

$$\frac{di}{dt} = \beta(t)si - (\delta + \mu)i, \quad (11)$$

$$\frac{dw}{dt} = 2\gamma(r - w) - \kappa\beta_0wi - \mu w, \quad (12)$$

where r is the density of individuals in the recovered class

$$r = 1 - s - i - w \quad (13)$$

and $\beta(t)$ is given by Eq. (3).

In the infinite population limit, the equations of the SIRIS model for the susceptible and infective densities are

$$\frac{ds}{dt} = \mu(1-s) - s[\beta(t)i_1 + \beta_0\eta i_2] + \gamma r, \quad (14)$$

$$\frac{di_1}{dt} = s[\beta(t)i_1 + \beta_0\eta i_2] - (\delta + \mu)i_1, \quad (15)$$

$$\frac{di_2}{dt} = \sigma\beta_0 r (i_1 + \eta i_2) - (\delta + \mu)i_2, \quad (16)$$

where

$$r = 1 - s - i_1 - i_2 \quad (17)$$

and $\beta(t)$ is given by Eq. (3). If $\beta_1 = 0$ the model has a trivial equilibrium and an endemic equilibrium where the densities of infectives and susceptibles lie between 0 and 1. The analytical computation of the endemic equilibrium values of i_1^* , i_2^* and s^* is straightforward but the expressions are lengthy and that is why we do not write them explicitly.

In the infinite population limit, the equations of the SIRSI model for the susceptible and infective densities are

$$\frac{ds_1}{dt} = \mu(1-s_1) - s_1[\beta(t)i_1 + \beta_0\eta i_2], \quad (18)$$

$$\frac{di_1}{dt} = s_1[\beta(t)i_1 + \beta_0\eta i_2] - (\delta + \mu)i_1, \quad (19)$$

$$\frac{ds_2}{dt} = \gamma r - \mu s_2 - \sigma\beta_0 s_2 (i_1 + \eta i_2), \quad (20)$$

$$\frac{di_2}{dt} = \sigma\beta_0 s_2 (i_1 + \eta i_2) - (\delta + \mu)i_2, \quad (21)$$

where

$$r = 1 - s_1 - i_1 - s_2 - i_2 \quad (22)$$

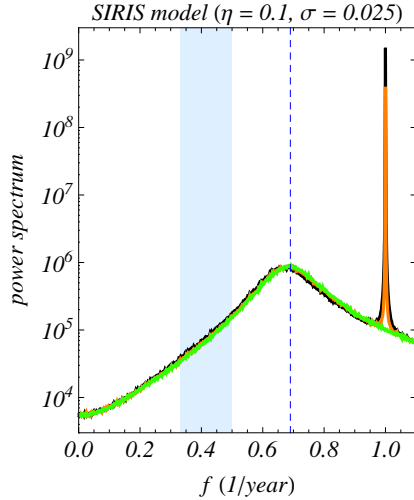


FIG. 1: (Color online) The dependence of the power spectrum of the SIRIS model on the amplitude of seasonal forcing β_1 . Parameters: $\beta_1 = 0$ [green (light gray)], 0.05 [orange (dark gray)], and 0.1 (black). The rest of the parameter values as for the black line in the left panel of Fig. 6 of the main text.

and $\beta(t)$ is given by Eq. (3). It can be shown that for $\beta_1 = 0$ the model has a trivial equilibrium and an endemic equilibrium where the densities of infectives and susceptibles lie between 0 and 1. As for the previous model, we do not give its explicit form.

A comparison of the equilibrium infective densities corresponding to the nontrivial fixed point as a function of β_0 for the five models is shown in Fig. 2 of the main text.

II. SIRIS MODEL FOR $\beta_1 \neq 0.05$

In the main text we presented the results for the SIRIS model for fixed $\beta_1 = 0.05$. Figure 1 shows the power spectra of the number of infective individuals from simulation for $\beta_1 = 0, 0.05, 0.1$. The stochastic peaks agree perfectly for all $\beta_1 \in [0, 0.1]$ and they are always far away from the shaded region. There is a remarkable resemblance of these spectra with those of the SIRS model for the same value of immunity waning rate (compare them with the black lines in Fig. 5 of the main text).

III. ANALYTICAL COMPUTATION OF THE DOMINANT FREQUENCY OF THE MULTIANNUAL PEAK

In this section we will describe how the dominant frequencies of the multiannual stochastic peaks in power spectra from simulations can be computed analytically. First, we note that in the three most interesting models which are the SIRWS, the SIR and the SIRSI model these frequencies are independent of $\beta_1 \in [0, 0.1]$ (see Fig. 7 and Fig. 8 of the main text). Thus, to predict the position of the stochastic peak in this parameter range it is sufficient to consider the unforced models with $\beta_1 = 0$ whose analysis is easier. The method we are going to use is usually referred to as the system size expansion first developed by van Kampen [2]. It has been successfully applied to several epidemiological models based on the S(E)IR or SIRS dynamics. We refer the reader to [3–5] for a more extensive discussion of the method in the context of unforced epidemiological models. The analysis of seasonally forced models can be found in [1, 6]. Here we will outline the most important steps of the calculations for the unforced SIRSI model because it has the largest number of classes.

The analytical treatment of the stochastic SIRSI model simulated using Gillespie’s algorithm starts with the construction of the master equation [2]. We describe the state of the system $l \equiv (l_1, l_2, l_3, l_4)$ by four numbers which are, sequentially, the number of susceptible S_1 , infective I_1 , susceptible S_2 , and infective I_2 individuals. The total population size N is fixed, that is why the number of recovered individuals R at any time is given by $N - l_1 - l_2 - l_3 - l_4$. The transition rates $\mathcal{T}_l^{l'}$ from the initial state l to the final state l' associated to the processes postulated in the diagram (e) of Fig. 1 of the main text can be written as follows:

1. Immunity waning: $R \xrightarrow{\gamma} S_2$.

$$\mathcal{T}_{l_1, l_2, l_3, l_4}^{l_1, l_2, l_3+1, l_4} = \gamma(N - l_1 - l_2 - l_3 - l_4). \quad (23)$$

2. Infection: $S_1 \xrightarrow{\bar{\lambda}_c} I_1$ and $S_2 \xrightarrow{\sigma \bar{\lambda}_c} I_2$, where $\bar{\lambda}^c = \beta_0(I_1 + \eta I_2)/N$.

$$\mathcal{T}_{l_1, l_2, l_3, l_4}^{l_1-1, l_2+1, l_3, l_4} = \beta_0 l_1 (l_2 + \eta l_4)/N, \quad (24)$$

$$\mathcal{T}_{l_1, l_2, l_3, l_4}^{l_1, l_2, l_3-1, l_4+1} = \sigma\beta_0 l_3(l_2 + \eta l_4)/N. \quad (25)$$

3. Recovery: $I_1, I_2 \xrightarrow{\delta} R$.

$$\mathcal{T}_{l_1, l_2, l_3, l_4}^{l_1, l_2-1, l_3, l_4} = \delta l_2, \quad (26)$$

$$\mathcal{T}_{l_1, l_2, l_3, l_4}^{l_1, l_2, l_3, l_4-1} = \delta l_4. \quad (27)$$

4. Birth and death: $R \xrightarrow{\mu} S_1$ and $S_1, I_1, S_2, I_2 \xrightarrow{\mu} R$.

$$\mathcal{T}_{l_1, l_2, l_3, l_4}^{l_1+1, l_2, l_3, l_4} = \mu N, \quad (28)$$

$$\mathcal{T}_{l_1, l_2, l_3, l_4}^{l_1-1, l_2, l_3, l_4} = \mu l_1, \quad (29)$$

$$\mathcal{T}_{l_1, l_2, l_3, l_4}^{l_1, l_2-1, l_3, l_4} = \mu l_2, \quad (30)$$

$$\mathcal{T}_{l_1, l_2, l_3, l_4}^{l_1, l_2, l_3-1, l_4} = \mu l_3, \quad (31)$$

$$\mathcal{T}_{l_1, l_2, l_3, l_4}^{l_1, l_2, l_3, l_4-1} = \mu l_4. \quad (32)$$

The master equation for the probability $\mathcal{P}(l, t)$ of having the system in state l at time t in the SIRSI model can be obtained by substituting Eqs. (23)-(32) into the general form for the master equation [2]:

$$\frac{d\mathcal{P}(l, t)}{dt} = \sum_{l' \neq l} \left[\mathcal{T}_{l'}^l \mathcal{P}(l', t) - \mathcal{T}_l^{l'} \mathcal{P}(l, t) \right]. \quad (33)$$

Given the initial and boundary conditions, the solution of Eq. (33) is equivalent to the full stochastic simulation of the model. The exact analytical solution of the master equation for the SIRSI model is not feasible but we can study its limit when the size of the system, N , becomes large [2]. The limit is formalized by representing the discrete variables l_k as a sum of two terms:

$$l_k(t) = N d_k(t) + \sqrt{N} x_k(t), \quad k = 1, \dots, 4. \quad (34)$$

The first term is the deterministic macroscopic term of the order of N and the second term are the fluctuations of the order of \sqrt{N} around the macroscopic state. To preserve the notation introduced in the main text we denote the functions $d_k(t)$

$$d_k(t) = \lim_{N \rightarrow \infty} \frac{l_k(t)}{N} \quad (35)$$

as the densities of susceptible individuals $s_1(t)$ for $k = 1$ and $s_2(t)$ for $k = 3$, and of infective individuals $i_1(t)$ for $k = 2$ and $i_2(t)$ for $k = 4$.

Substituting Eq. (35) into Eq. (33) results in an equation for the probability distribution $\Pi(x, t)$ of the fluctuations $x \equiv (x_1, x_2, x_3, x_4)$ around the deterministic trajectory in which terms of different orders in $1/\sqrt{N}$ can be identified. After collecting and equating terms of the leading order one obtains the deterministic SIRSI equations with $\beta_1 = 0$ [see Eqs. (19)-(22)]. The same procedure for terms of the next to leading order gives rise to a linear Fokker-Plank equation in the variable x [2]:

$$\frac{\partial \Pi(x, t)}{\partial t} = - \sum_{k,j} A_{kj}(t) \frac{\partial (x_j \Pi(x, t))}{\partial x_k} + \frac{1}{2} \sum_{k,j} B_{kj}(t) \frac{\partial^2 \Pi(x, t)}{\partial x_k \partial x_j}, \quad k, j = 1, \dots, 4. \quad (36)$$

In Eq. (36), $\mathbf{A}(t)$ is the Jacobian of the deterministic SIRSI model with $\beta_1 = 0$

$$\mathbf{A}(t) = \begin{pmatrix} -g - \mu & -\beta_0 s_1 & 0 & -\beta_0 \eta s_1 \\ g & \beta_0 s_1 - (\delta + \mu) & 0 & \beta_0 \eta s_1 \\ -\gamma & -\sigma \beta_0 s_2 - \gamma & -\sigma g - (\gamma + \mu) & -\sigma \beta_0 \eta s_2 - \gamma \\ 0 & \sigma \beta_0 s_2 & \sigma g & \sigma \beta_0 \eta s_2 - (\delta + \mu) \end{pmatrix} \quad (37)$$

and $\mathbf{B}(t)$ is the symmetric cross correlation matrix computed directly from the expansion

$$\mathbf{B}(t) = \begin{pmatrix} g s_1 + \mu(1 + s_1) & -g s_1 & 0 & 0 \\ -g s_1 & g s_1 + (\delta + \mu) i_1 & 0 & 0 \\ 0 & 0 & \gamma r + (\sigma g + \mu) s_2 & -\sigma g s_2 \\ 0 & 0 & -\sigma g s_2 & \sigma g s_2 + (\delta + \mu) i_2 \end{pmatrix}, \quad (38)$$

where

$$g = \beta_0 (i_1 + \eta i_2) \quad (39)$$

and

$$r = 1 - s_1 - i_1 - s_2 - i_2. \quad (40)$$

To compute the power spectrum of the fluctuations it is useful to use the Langevin equation [2] associated with Eq. (36) which reads as

$$\frac{dx_k(t)}{dt} = \sum_j A_{kj}(t) x_j(t) + L_k(t), \quad k, j = 1, \dots, 4, \quad (41)$$

where $L_k(t)$ are Gaussian noise terms with zero mean

$$\langle L_k(t) \rangle = 0 \quad (42)$$

and with the correlator

$$\langle L_k(t)L_j(t') \rangle = B_{kj}(t)\delta(t-t'). \quad (43)$$

Finally, since we are interested in the fluctuations in the stationary state we evaluate the matrices $\mathbf{A}(t)$ and $\mathbf{B}(t)$ at the endemic steady state $(s_1^*, i_1^*, s_2^*, i_2^*)$ of the deterministic SIRSI equations (with $\beta_1 = 0$). The power spectrum of the fluctuations for infectives I_1 around the endemic equilibrium of the unforced SIRSI model is defined as $P_{I_1}(\omega) \equiv \langle |\tilde{x}_2(\omega)|^2 \rangle$. Figure 2 shows P_{I_1} as a function of frequency measured in the units of $f = \omega/2\pi$ for the parameter values used in Fig. 8 of the main text. As before, the blue shaded region corresponds to multi-annual periods in the range 2 to 3 years where the multiannual peaks of the spectra computed from London and Ontario data are located. The frequency corresponding to the center of the shaded region, f_c , is thus $5/12 \text{ year}^{-1}$. The frequency of the maximum of the spectrum, f_{peak} , is $0.409401 \text{ year}^{-1}$. We used this value to draw the dashed blue vertical line in the right panel of Fig. 8 of the main text.

As described in the main text we also studied the properties of the spectra for the unforced SIRSI model for other parameter values. For fixed γ , we considered in the interval $(0, 1)$ nine equally spaced values and constructed a grid of 81 points in the (η, σ) space. Figure 3 shows the values of f_{peak} on this grid for $\gamma = 1/20 \text{ year}^{-1}$. We further calculated the number of spectra N_{target} for which

$$\frac{1}{3} \leq f_{peak} \leq \frac{1}{2} \quad (44)$$

and the number of spectra N_0 for which

$$\frac{f_c}{1.05} \leq f_{peak} \leq \frac{f_c}{0.95}. \quad (45)$$

The former gives the total number of spectra in the target region, and the latter gives the number of spectra with periods within 5% of the period corresponding to the center of the target region. The results are summarized in Table I for three different values of γ .

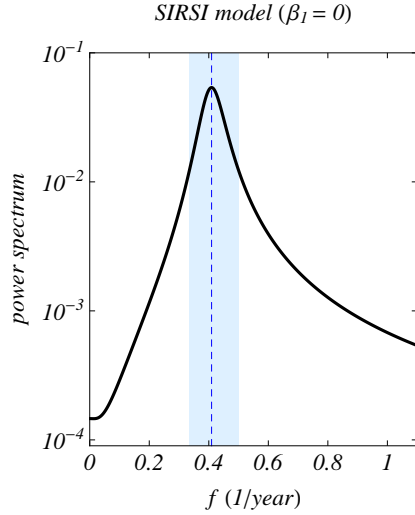


FIG. 2: (Color online) Analytical power spectrum of the unforced SIRSI model for parameter values used in the right panel of Fig. 8 of the main text. The shaded region marks the frequencies between $1/3 \text{ year}^{-1}$ and $1/2 \text{ year}^{-1}$ and the dashed blue vertical line corresponds to the frequency of the maximum of the spectrum.

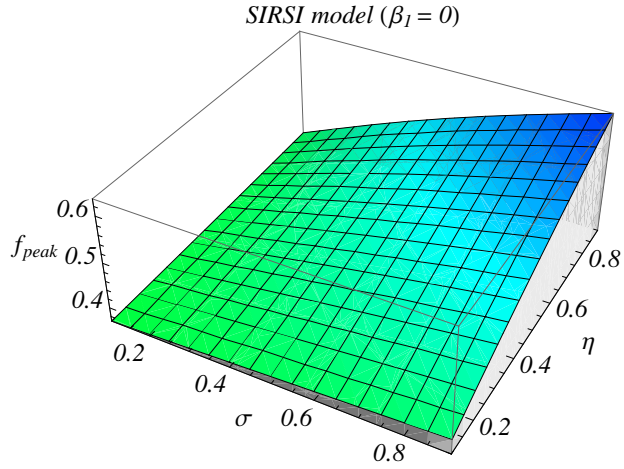


FIG. 3: (Color online) The frequency of the maximum of the analytical power spectrum of the unforced SIRSI model as a function of η and σ . The plot is made for $\gamma = 1/20 \text{ year}^{-1}$. This value was used in Fig. 2 of this section and in the middle and right panels of Fig. 8 of the main text.

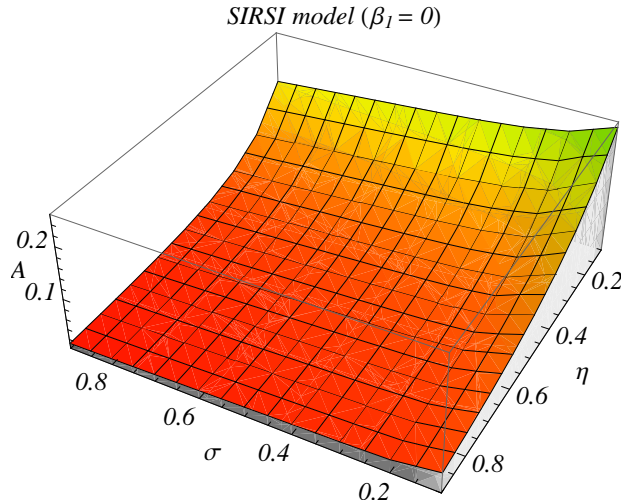


FIG. 4: (Color online) The amplitude A of the peak of the analytical power spectrum of the unforced SIRSI model as a function of η and σ . The plot is made for $\gamma = 1/20 \text{ year}^{-1}$.

$\gamma \text{ (year}^{-1}\text{)}$	1/40	1/20	1/10
N_{target}	78	62	43
N_0	28	20	16
A_{min}	0.0602494	0.0280422	0.0159649
A_{max}	0.165027	0.166171	0.123987

TABLE I: Values for the quantities used in the comparison and description of the spectra for the unforced SIRSI model in the (η, σ) space and different values of γ .

Another quantity of interest in the description of power spectra is the amplitude of the peak A . Figure 4 shows the amplitude for the same 81 points with $\eta, \sigma \in (0, 1)$ and $\gamma = 1/20 \text{ year}^{-1}$. The value of A is particularly interesting for the N_0 spectra with their peaks in center of the target region. In Table I we give the maximum and the minimum amplitude among these N_0 spectra for different values of γ . The amplitude of the peak plotted in Fig. 2 of this section is 0.0538342, in the middle of the range of A when $\gamma = 1/20 \text{ year}^{-1}$.

This study of the unforced SIRSI model is applicable to the case $\beta_1 \neq 0$, because we observe that the amplitude of the stochastic peak does not change for the seasonally forced

SIRSI model.

The conclusion of this section is that the SIRSI model's spectrum is robust with respect to variation of all free parameters. On one hand, there is a large region of parameter space where the dominant frequency of the stochastic peak is centered in the region of interest. On the other hand, these spectra have some variability in the peak's amplitude for different values of η , σ and γ .

-
- [1] Rozhnova, G. & Nunes, A. 2010 Stochastic effects in a seasonally forced epidemic model. *Phys. Rev. E* **82**, 041906.
 - [2] van Kampen, N. G. 1992 *Stochastic processes in physics and chemistry*. Amsterdam, The Netherlands: Elsevier.
 - [3] Alonso, D., McKane, A. J. & Pascual, M. 2007 Stochastic amplification in epidemics. *J. R. Soc., Interface* **4**, 575-582.
 - [4] Rozhnova, G. & Nunes, A. 2009 Fluctuations and oscillations in a simple epidemic model. *Phys. Rev. E* **79**, 041922.
 - [5] Black, A. J. & McKane, A. J. 2010 Stochasticity in staged models of epidemics: quantifying the dynamics of whooping cough. *J. R. Soc., Interface* **7**, 1219–1227.
 - [6] Black, A. J. & McKane, A. J. 2010 Stochastic amplification in an epidemic model with seasonal forcing. *J. Theor. Biol.* **267**, 85–94.